

Characterization and analysis of biochar derived nano materials for application of Cd(II) removal

Zhaoyang Luo*, Ping Zhang, Jun Duan

Dazhou Vocational and Technical College, Dazhou 635001, China, email: zhaoyang8540@163.com (Z.Y. Luo)

Received 30 November 2022; Accepted 27 September 2023

ABSTRACT

Biochar-based nanomaterials are an efficient and economical adsorption material, often used to adsorb and remove heavy metals in sewage. In this study, eucalyptus biochar nanomaterials were produced by pyrolysis as a carbon precursor and modified with potassium penetrant (KBC) to improve its adsorption performance for Cd removal. Various characterization techniques have been used to fully characterize and analyze the physical and chemical properties of KBC. The adsorption kinetics, thermodynamics and adsorption isotherms of KBC on Cd(II) ions and the effects of various reaction parameters (pH, adsorbent dosage, adsorption time, temperature and initial concentration) on the adsorption capacity and removal rate were evaluated. The results show that the best adsorption capacity of KBC for Cd(II) is 31.050 mg/g, under the best conditions (pH = 5, dosage = 0.08 g, time = 6 h, temperature 25°C and initial concentration = 50 mg/g-L). The adsorption process follows the pseudo-second-order kinetic model and the isothermal Langmuir adsorption model. This model is based on a single layer adsorbed on a uniform surface and absorbs heat spontaneously under physical and chemical action. The adsorption mechanism of Cd(II) is mainly through complexation, oxidation and cation- π -electron interaction to adsorb oxygen-containing and manganese-containing KBC groups. Potassium permanganate surface-modified eucalyptus biochar proved to be an effective method to deal with heavy metal pollution.

Keywords: Eucalyptus biochar; Potassium permanganate; Modification; Adsorption; Cd(II)

1. Introduction

With the continuous exploitation of energy resources by social development, more and more industries such as mining, beneficiation, electroplating plants are emerging, resulting in groundwater and surface water pollution often containing a variety of heavy metal pollutants. As a typical heavy metal, cadmium has strong corrosion resistance and is widely used in electroplated steel, iron, copper and other metals. The cadmium emissions of different industries vary greatly.

Cadmium cannot be degraded naturally after entering water bodies, it is easy to accumulate and gradually transfer and accumulate in organisms through the food chain

[1]. Therefore, after cadmium enters the human body, it is very harmful to the kidneys and affects renal tubular function. When cadmium reaches a certain level, renal tubular disease will occur. Long-term intake of cadmium-containing rice and other foods can also cause severe bleeding and renal failure [2].

The most important treatment methods for wastewater containing cadmium are currently electro-flocculation [3], chemical precipitation [4], adsorption [5] and ion exchange [4,6] and membrane separation processes [7]. In recent years, however, due to its better mechanical properties, functional groups and high surface area, biochar has become more and more popular as an adsorbent for the adsorption of heavy metals.

* Corresponding author.

As the raw material of biochar, agricultural and forestry waste has the advantages of large source and low cost. Converting agricultural and forestry wastes into biochar is an environmentally friendly waste treatment method. Eucalyptus has a short growth cycle and a fast growth rate. It is widely used in papermaking and wood processing and has good economic value.

Eucalyptus is like a tall tree, rich in cellulose, hemicellulose and lignin [8]. The biochar obtained by pyrolysis has a good pore structure and abundant functional surface groups. Eucalyptus is planted in large quantities in Guangxi, with diverse sources, and has a huge potential for biochar production.

Due to the different materials and methods of biochar production, biochar has the disadvantages of low adsorption capacity, poor selective adsorption capacity, and poor treatment of high-concentration heavy metal wastewater [9], and it is difficult to directly use biochar large-scale. In order to improve the adsorption performance of biochar, researchers used various methods to modify biochar to improve the pore structure and surface area [10] and increase the number of functional groups on the surface of biochar [11].

Manganese oxide has a high specific surface area, a rich microporous structure, many adsorption sites, and low toxicity. Although manganese oxide as an adsorbent has a good adsorption effect on heavy metals, it also has problems such as weak mechanical strength, easy polymerization in solution, complex dispersion, and low adsorption efficiency [12]. Therefore, to solve these problems, it is necessary to find a substrate suitable for loading and attaching manganese oxide particles [13].

As a particular adsorbent, biochar is inexpensive and readily available, has a large surface area and good pore structure, promotes loading of manganese oxides, and can dissolve traces of polymerized manganese oxides in water [14]. In addition, the combination of manganese oxide and biochar also helps to improve the adsorption efficiency of biochar [15,16].

In this paper, a new eucalyptus biochar adsorbent nanomaterials (KBC) was synthesized. This study will provide a theoretical basis and reference to cadmium wastewater treatment and will open up new uses for land and forestry waste.

2. Materials and methods

2.1. Preparation of modified eucalyptus biochar nanomaterials

Eucalyptus green material was purchased from eucalyptus forest, China, and the main reagents were cadmium nitrate and potassium permanganate. The eucalyptus wood was chopped and washed, dried in an oven at 60°C for 12 h, then taken out, chopped, filtered through a 60-mesh screen to obtain a sample, and sealed. Place 10 g of the sample in a 50 mL crucible, put it in a muffle furnace, and raise the temperature to 600°C at a heating rate of 5°C/min, and keep it at a constant temperature for 2 h. Place the washed carbon sample in a 50 mL polyvinyl chloride centrifuge tube to separate the solid and liquid. The resulting biochar was labeled (BC) and dried in an oven at 60°C for 12 h, then sealed and stored.

BC is modified with potassium permanganate, and its preparation method is similar to that of Sun et al. [17]. In short, take 50 mL of 0.1 mol/L potassium permanganate solution and pour it into a 100 mL beaker containing 2.0 g BC, mix thoroughly, and then put it in a magnetic stirrer and stir at 500 rpm for 12 h. 50°C, rinse with deionized water, repeat the above steps 3 times, put the washed labeled KBC nanomaterials into an oven at 60°C for 12 h, dry and seal for storage.

2.2. Characterization of nanomaterials

The structural analysis of the nanomaterials is based on the analysis of the specific analysis and the specific analysis of the Brunauer–Emmett–Teller (BET). Engineer Zort Thermesch Scanning Electron Microscope SU5000 SEM and energy-dispersive X-ray spectroscopy (EDS; Hitachi, Japan) have good results in terms of analysis and EDS firm analysis and Uewerflächelementer. The X'PertPRO XRD diffractometer (Panaco, The Netherlands) is used to determine the size of the crystal structure. Analytical information on the elemental determination of the X-ray photoelectron spectroscopy of the ESCALAB 250Xi (American Thermoelectric Company).

2.3. Adsorption experiments

Cd(II) adsorption is affected by the adsorbent by various factors such as the dose and pH of the adsorbent. 50 mL of 50 mg/L Cd(II) solution was taken into a centrifuge tube at 25°C and the adsorbent dose and pH factors were applied. pH effect experiment: 80.0 mg of adsorbent was injected and the pH was adjusted to 2–7. The adsorbent dosing amount affected the experiment: pH was adjusted to 5 and the dosing amounts were set to 0.02–0.14 g. The dosing of the adsorbent affected the experiment: the pH was adjusted to 5 and the dosing amounts were set to 20.0, 40.0, 60.0, 80.0, 100.0, 120.0 and 140.0 mg. The centrifuge tubes were kept in a constant temperature water bath shaker and shaken for 24 h. The mass concentration of Cd(II) in the filtrate was determined. The amount of Cd(II) adsorption and removal rate in solution were calculated according to Eqs. (1) and (2).

$$q = \frac{(c_0 - c_t)V}{m} \quad (1)$$

$$\eta(\%) = \frac{(c_0 - c_t)}{c_0} \times 100 \quad (2)$$

where c_0 and c_t are the concentrations (mg/L) of the Cd(II) solution at the initial moment and at time t , respectively; m is the mass of the adsorbent and V (L) correspond to the volume of the solution.

2.4. Dynamics and isotherm experiments

For the adsorption kinetics experiment, 50 mL of 50 mg/L Cd(II) solution was taken and 80.0 mg of KBC was added. A time gradient from 5 to 1,440 min was determined, and the mass concentration of Cd(II) after adsorption was measured. Experimental adsorption data were presented

using a pseudo-expression model, a pseudo-second-order kinetic model, a single-particle inner membrane diffusion model [Eqs. (3)–(5)].

$$\ln(q_e - q_t) = \ln q_e - k_1 t \tag{3}$$

$$\frac{t}{q_t} = \frac{1}{k_2 q_e^2} + \frac{t}{q_e} \tag{4}$$

$$q_t = k_{di} t^{1/2} + c_i \tag{5}$$

where t : adsorption time (min), q_e and q_t is the absorption capacity (mg/g) at t and equilibrium, respectively, k_1 (min^{-1}) is the pseudo-first-order rate constant, k_2 is the pseudo-second-order (g/mg·min), c_i is the constant with respect to the boundary layer thickness (mg/g).

Nettle adsorption isothermal experimenters were given 50.0 mL of Cd(II) solutions from 50.0 to 400.0 mg/L, 50.0 mL, 80.0 mg of KBC and the reaction was run for 24 h. Experimental isothermal data were analyzed using the Langmuir model [Eq. (6)]. The Friendly model [Eq. (7)]:

$$\frac{c_e}{q_e} = \frac{c_e}{q_m} + \frac{1}{q_m K_L} \tag{6}$$

$$\ln q_e = \ln K_F + \frac{1}{n} \ln c_e \tag{7}$$

$$R_L = \frac{1}{1 + K_L c_0} \tag{8}$$

where c_e is the concentration of the solution at adsorption equilibrium, mg/L, q_e is the equilibrium adsorption amount, (mg/g), q_m is the maximum adsorption content (mg/g), K_L ; Langmuir-Constant (L/mg); further describing the absorption characteristics of the Langmuir model, K_F was the friendly adsorption constant [(mg/g)(mg/L)^{1/n}] and the absorption intensity (dimension) of the n -friendly isothermal model.

3. Results and discussions

3.1. Characterization of biochar nanomaterials

The specific surface area of biochar nanomaterials, its pore volume, and pore size were greatly altered after modification by potassium permanganate (Table 1). The specific surface area and the total pore volume of the biochar

Table 1
Pore structure and surface area of biochar and KBC nanomaterials

Material types	BET surface area (m ² /g)	Total hole volume (cm ³ /g)	Average pore size /nm
Biochar	401.8	0.26	2.5
KBC	27.3	0.06	8.3

decreased, and the average pore size increased. Changes in the pore structure are associated with the loading of manganese oxides and their strong oxidation with potassium permanganate, which blocks the pore structure on the biochar surface and reduces the biochar surface and pore capacity [18], and due to strong oxidation, some nanopore structures disappear, converting nanopores into mesopores of larger pore size [17].

The scanning electron microscopy (SEM) and EDS maps of BC and KBC are shown in Fig. 1, it is concluded that the surface of the BC is smooth and the pore capacity is obvious. After the change, the KBC surface becomes rough and the particle cleaners and pore structures are filled with manganese oxides. Fig. 1e–f shows that BC consists mainly of elemental carbon and oxygen. After the change, manganese and potassium elements form in the KBC, while the amount of carbon elements decreases and the oxygen elements increase.

Fig. 2 shows the biochar X-ray diffraction (XRD) model. BC has several diffraction peaks at 2°, 22.8°, 29.4°, and 39.50°, respectively. The biochar consists mainly of uncharacteristic carbon [19]. The intensity of the large band corresponding to amorphous carbon BC was significantly attenuated after the change [19]. This indicates that there is a chemical interaction between the biostone and potassium permanganate in the modification process. KBC produces manganese oxides in the form of MnO₂ at 13.52°, 24.01°, 36.79°, and 67.22°, respectively [20]. This indicates that the BC surface is successfully charged with manganese oxides after modification with potassium permanganate, which has a good modifying effect on the eucalyptus biochar [21].

Fig. 3a shows the full spectrum of biochar is shown, indicating the major BC elements C, and the presence of O. Mn elements on the KBC surface indicates that manganese oxides were well attached to the biochar surface. After the adsorption of Cd(II) on KBC, elemental cadmium appears on the surface. This shows that Cd(II) was successfully adsorbed on the biostone during the adsorption process. After the change, the O1s peaks increased significantly and the quantity of oxygen elements increased significantly. However, the maximum intensity of the manganese element did not change significantly, proving that the adsorption process did not affect the manganese oxides loaded into the biochar. and was able to maintain a stable structure during the adsorption process, which was profitable for a long time with a modified biochar that was consistent with the results of the XRD analysis (Fig. 3b) a narrow spectrum of manganese elements is shown. The diffraction peaks at 653.83 and 642.32 eV for the manganese element charged on the BC surface correspond to Mn2p_{1/2} and Mn2p_{3/2}, indicating that both tetravalent and trivalent manganese oxides are charged on the KBC surface and manganese oxides are tetravalent dominant [22]. Narrow O1s spectra before and after modification and adsorption are shown in Fig. 3c and d. And the surface peaks at the BC surface can be attached to the four peaks, and the corresponding peaks correspond to the functional group Mn–O, Mn–OH, C–OH, and H₂O, which can provide more adsorption sites for absorption. from Cd(II). After Cd(II) adsorption, the peak areas of C–OH and Mn–OH decrease and Mn–O increases. This indicates that C–OH is involved in the adsorption of Cd(II) during

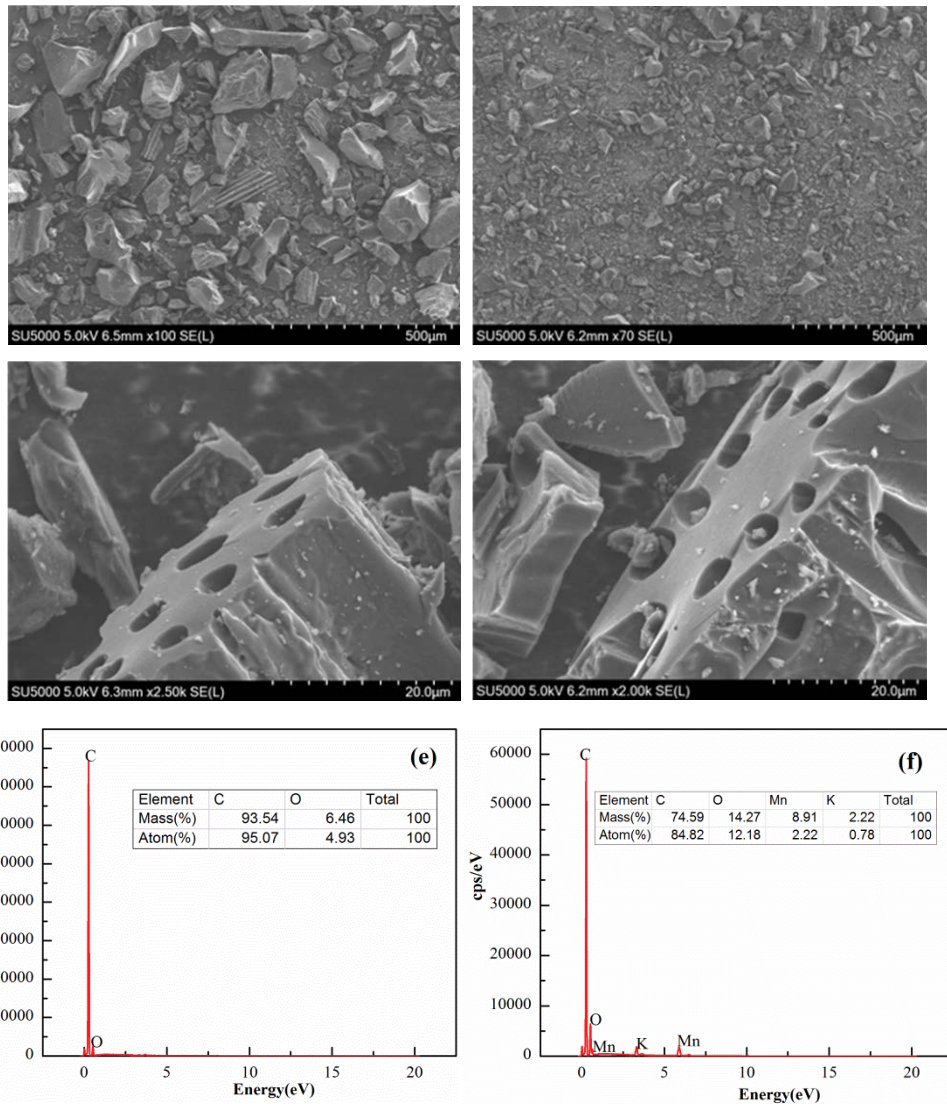


Fig. 1. Scanning electron microscopy-energy-dispersive X-ray spectroscopy images of biochar and KBC: (a) biochar-scanning electron microscopy, (b) KBC-scanning electron microscopy, (c) biochar-scanning electron microscopy, (d) KBC-scanning electron microscopy, (e) biochar-energy-dispersive X-ray spectroscopy, and (f) KBC-energy-dispersive X-ray spectroscopy.

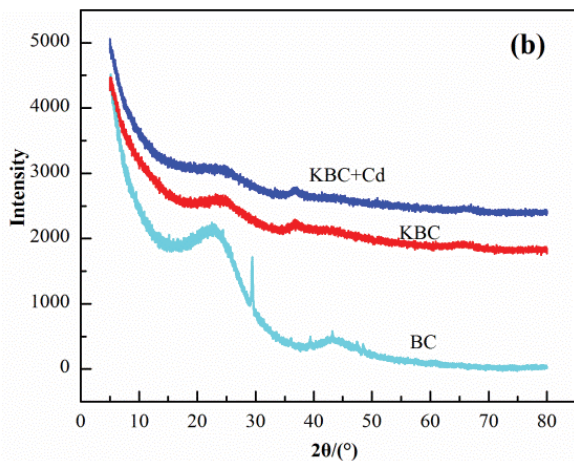


Fig. 2. Nanomaterials X-ray diffraction graph.

the adsorption process. The increased Mn–O and biochar content is associated with an increase in Cd–O on the KBC surface, suggesting that –O–Cd–O-bidentate complexes are formed on the biochar surface during the adsorption process [6]. However, the reduced H₂O content indicates that this molecule is adsorbed on the KBC surface and is also involved in the adsorption process of the Cd(II) process. Water molecules also influence the adsorption process to some extent [6]. From the narrow spectrum of Cd3d Fig. 3e, the binding energy values of the two Cd3d peaks after adsorption were 417.77 eV at Cd_{3/2} and 415.16 eV at Cd_{5/2} (II).

Interactions with oxygen-containing functional groups. Fig. 3 reflects the change in C₁ during the adsorption process. The C₁ peaks at 284.8 and 292.78 eV correspond to the functional groups C–C and O=C–O. The intensity of the C₁ peak at 292.78 eV decreased significantly after Cd(II) adsorption, which proves that the interaction of O=C–O with Cd(II) also exists during the adsorption process.

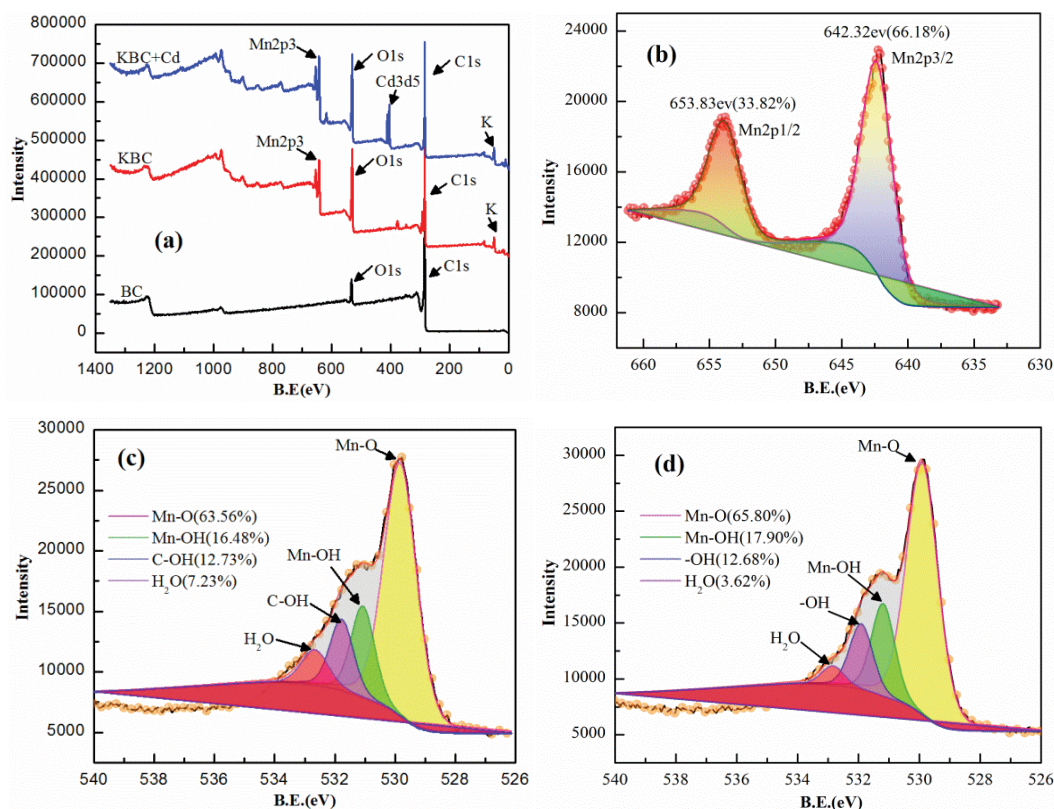


Fig. 3. X-ray photoelectron spectrum of biochar: (a) shows the full spectrum of biochar, (b) shows the narrow spectrum of manganese element, (c) shows the narrow spectrum of O1s before and after modification, and (d) shows the narrow spectrum of O1s before and after adsorption.

Biochar is converted to carbon by pyrolysis at high temperatures, characterized by irregular graphene micro-crystals. Especially in biomarkers, it contains many polar π electrons [23]. In this study, the eucalyptus tree, which is rich in cellulose and hemicellulose, as well as the biotone obtained by polymerization at 600°C for 2 h, is rich in polarized π electrons [15], that is, metal and die π -electronic communication takes place with the adsorption of Cd(II).

3.2. Effect of reaction conditions on the adsorption effect

Using BC and KBC, Cd(II) was adsorbed under the same conditions under experimental conditions (adsorbent dose 0.08 g, pH 5, initial Cd(II) concentration 50 mg/L, solution volume 50). The concentration of Cd(II) in mL (mL, temperature 25°C and adsorption time 24 h) and the concentration of Cd(II) in the solution were checked by ICP after the reaction, and the amount of adsorbed Cd(II) was calculated using the Eq. (1). The amount of adsorption of Cd(II) was calculated. The adsorption of Cd(II) BC under the same conditions was 26.438 mg/g, but the adsorption of Cd(II) KBC (31.050 mg/g) was higher than that of BC. This indicates that the adsorption of Cd(II) KBC increased after modification.

In Fig. 4a, the effect of adsorbent dose on the adsorption of Cd(II) is shown. When the dose of KBC was increased from 20.5 to 40.5 mg, the amount of Cd(II) adsorbed by KBC decreased sharply from 83.67 to 46.38 mg/g. When

the dose exceeded 40.5 mg, the adsorption amount slowly decreased to 18.75 mg/g. The decrease in Cd(II) adsorption by KBC was due to the limited amount of Cd(II) in solution and the difficulty in obtaining it. Increase the adsorbent dose to saturate the adsorption sites of KBC [24]. Increasing the KBC dose from 20.0 to 80.0 mg increased the percentage of Cd(II) clearance with KBC from 34.86% to 99.45%. The Cd(II) KBC clearance rate increases from 99.45% to 99.96% when the dose exceeds 80.0 mg and the clearance rate is stable. The removal rate is due to the adsorption sites provided by the adsorbent, which is used to adsorb Cd(II) in the solution when the amount of KBC administered to the Cd(II) solution increases from 20.5 to 80.5 mg. The number of effective active adsorption sites has increased and the removal rate has increased. Above the dose of 80.5 mg, no increase in Cd(II) removal was seen, providing a more efficient adsorption site associated with large amounts of adsorbent in solution and partial aggregation of KBC in solution. It became difficult. For Cd(II), considering the effect of KBC removal on Cd(II) and the complete use of the adsorbent, 80.5 mg KBC and 50.50 mL Cd(II) solution were selected as the adsorbent dose for the experiment.

The pH affects both the surface chemistry of the biochar and the form of Cd(II) present in solution. The effect of pH on Cd(II) KBC adsorption in Fig. 4b shows that Cd(II) KBC removal and adsorption increased from 18.20% and 5.78 mg/g to 97.55%. And 31.80 mg/g, if the pH of the solution increased from 2.0 to 5.0. Removal of Cd(II) with

KBC achieves stability when the pH of the solution exceeds 5.0 ± 0.1 . Fig. 4c shows the distribution of Cd(II) analyzed using a model built with Visual MINTEQ software. The predominant form of Cd(II) present in solution is Cd^{2+} which is present in more than 96% solution in the pH range 2.1 to 7.2. The adsorption of Cd(II) by KBC in solution depends on the interaction between KBC and Cd^{2+} . The removal effect at low pH 2.1 is due to the high amount of H^+ in the low pH solution. The main form of Cd(II) is Cd^{2+} , with competition between H^+ and Cd^{2+} during adsorption of KBC and charge repulsion between KBC and Cd^{2+} [25]. As the pH of the solution increased, protonation on the biochar surface decreased, competitive adsorption with H^+ decreased, and the KBC removal efficiency for Cd(II) increased. As shown in the pH diagram after adsorption of Cd(II) in Fig. 4d, the pH of the solution increased after adsorption. This may be due to ion exchange between biochar and Cd(II) present in the adsorption process [26].

Fig. 4e shows the influence of the adsorption time on the adsorption of Cd(II) KBC nanomaterials. The adsorption of KBC on Cd(II) was divided into three stages. The adsorption proceeds rapidly during the first 61 min, and the Cd(II) removal rate was 96.42% with an adsorbed amount of 31.43 mg/g of a Cd(II) solution, and the adsorption process was a rapid adsorption stage. During 60–242 min, the adsorption of Cd(II) KBC slowed and the adsorption amount of Cd(II) KBC increased to 31.80 mg/g at a removal rate of

97.19%. After the rapid adsorption, the adsorption sites on the surface of the adsorbent were occupied by a large amount of Cd(II), the binding rate of KBC and the Cd(II) solution decreased, and the adsorption process gradually tends to be saturated. When the adsorption time reaches 361 min, the adsorption becomes saturated, and the adsorption amount and the removal rate become maximum.

The experimental data were adapted and analyzed with models of intraparticle diffusion, the kinetics of pseudo-first-order and pseudo-second-order [26]. As in Table 2 and Fig. 5a & b, the theoretical equilibrium adsorption amount of 30.98 mg/g for adsorption of Cd(II) by KBC, calculated with a pseudo-second-order kinetic model, is the experimental result of 30.87 mg almost similar /g for Cd(II). Therefore, the pseudo-second-order kinetic model can better reflect the adsorption of Cd(II) KBC. From the results of the adaptation of the diffusion model to the inner particle membrane in Fig. 5e it can be seen that the adsorption of Cd(II) by KBC comprises three steps. In the initial stage, Cd(II) diffuses from solution to the KBC surface, and q_t changes rapidly with time, the stage of rapid adsorption. The second stage is the intraparticle diffusion of Cd(II) into the KBC. The third stage is the equilibrium stage caused by the saturation of the KBC adsorption center. The c_i values for the three stages of Cd(II) adsorption by KBC are not zero and the k_{di} values for the three stages gradually decrease, suggesting that adsorption of Cd(II) by KBC is not only

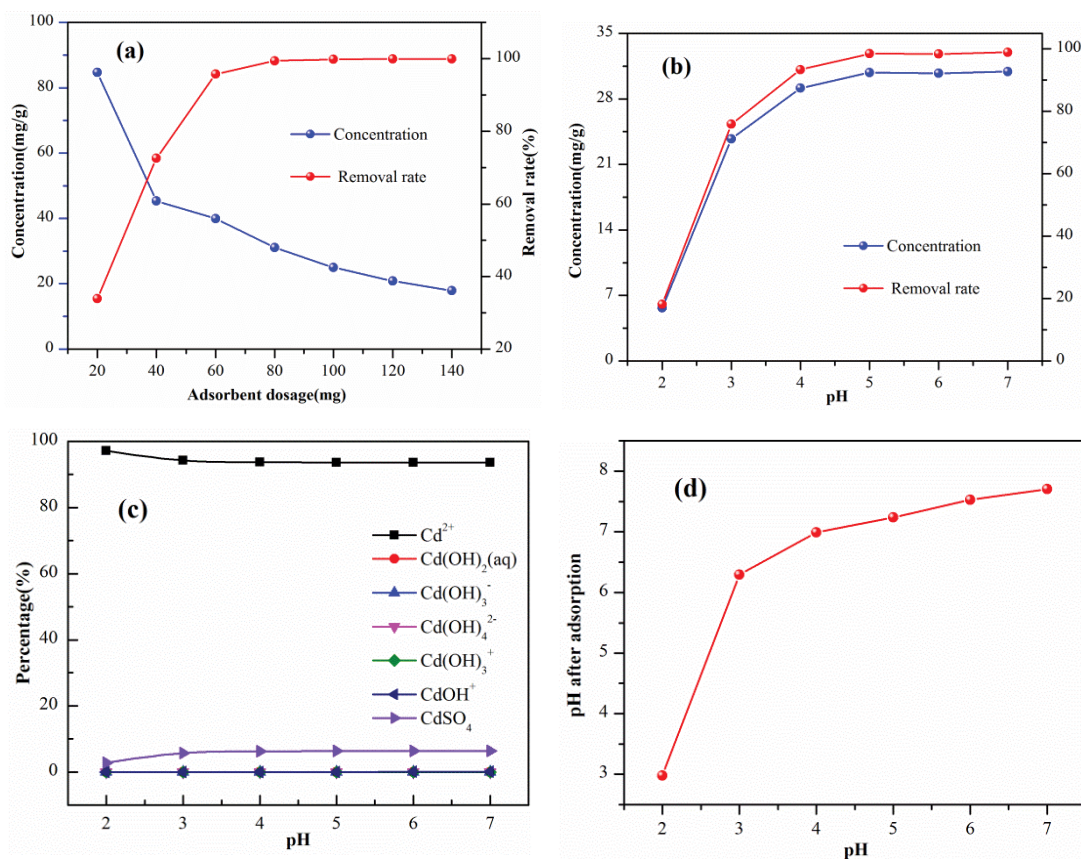


Fig. 4. Effect of reaction conditions on the adsorption effect: (a) effect of KBC dosing on Cd(II), (b) effect of pH on the adsorption of Cd(II) by KBC, (c) distribution of Cd(II) at different pH, and (d) pH diagram after adsorption of Cd(II).

Table 2
Kinetic model of Cd(II) adsorption by KBC and diffusion model of the inner membrane of the particles

Adsorbent	Experimental values	Pseudo-level dynamics	Pseudo-secondary dynamics	Granular spreading model		
Cd(II)	$q_{e,exp} = 30.970$ (mg/g)	$q_e = 1.330$ (mg/g)	$q_e = 30.980$ (mg/g)	$K_{id1} = 0.45$	$K_{id2} = 0.03$	$K_{id3} = 0.00$
		$k_1 = 0.003$ (min^{-1}) $R^2 = 0.825$	$k_2 = 0.028$ (g/mg·min) $R^2 = 1.000$	$C_1 = 27.26$ $R_1^2 = 0.92$	$C_2 = 30.30$ $R^2 = 0.93$	$C_3 = 30.69$ $R_{32} = 0.98$

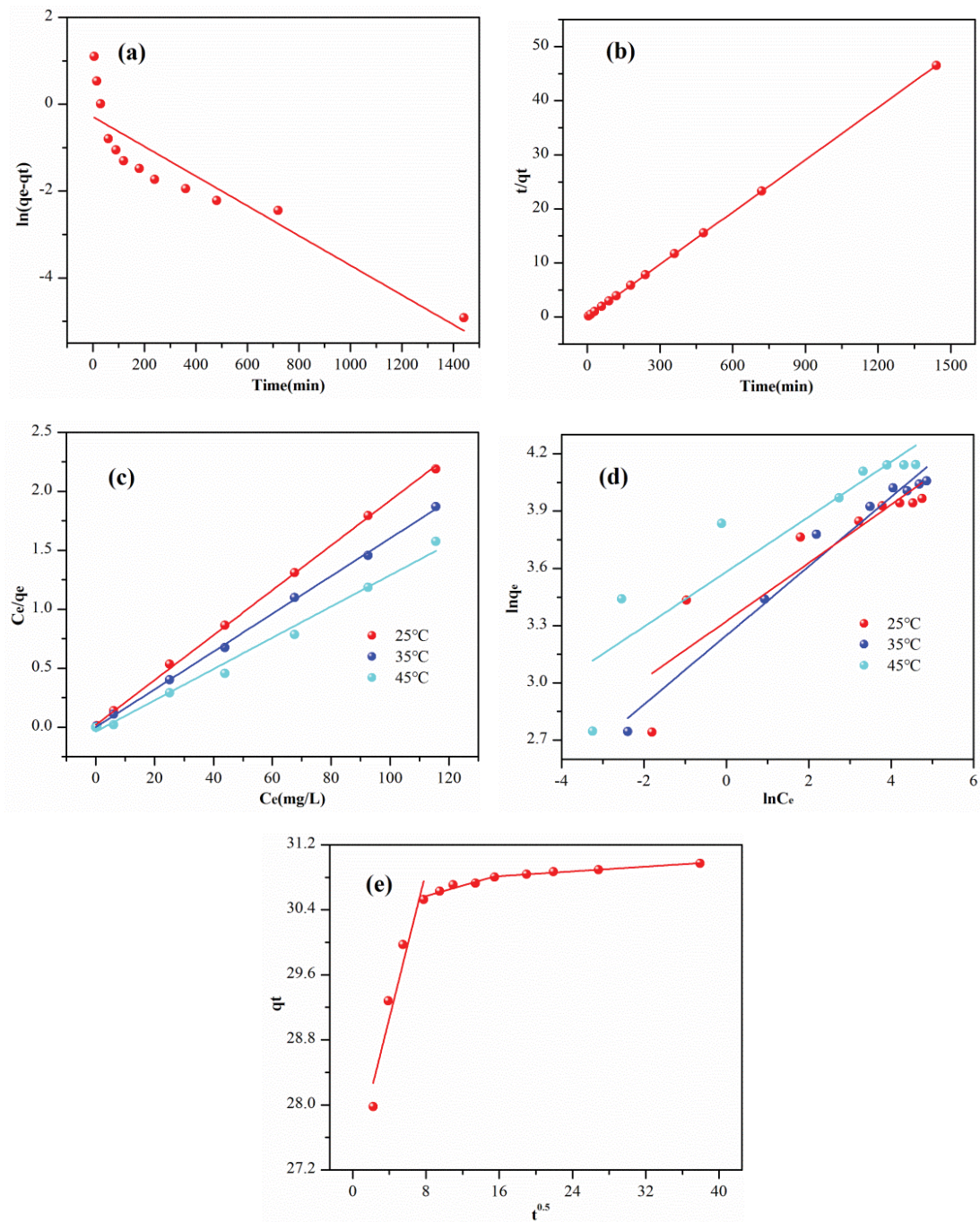


Fig. 5. Model fitting diagram of adsorption effect: (a) pseudo primary kinetic model fit, (b) pseudo secondary kinetic model fit, (c) Langmuir, (d) Freundlich, and (e) particle inner film diffusion model fitting.

Table 3
Parameters of the Langmuir model Freundlich model fit for Cd(II) adsorption by KBC

Adsorbent	T	Experimental values		Langmuir		Freundlich		
		q_e (mg/g)	q_{max} mg/g	K_L (L/g)	R^2	K_f	N	R^2
Cd(II)	25°C	52.8	52.7	0.75	0.99	27.7	6.5	0.83
	35°C	57.8	57.8	0.75	0.99	25.7	5.5	0.97
	45°C	63.0	67.07	0.79	0.99	35.9	6.9	0.83

internal dissemination is limited. Particles, but other effects collectively affect the adsorption process [27].

Fig. 4f shows the effect of the initial concentration on Cd(II) adsorption of KBC nanomaterials. The increase in Cd(II) for KBC increased with increasing initial concentration of Cd(II) up to 126 mg/L. In contrast, the Cd(II) uptake of KBC reached saturation when the initial concentration of Cd(II) 126 was above mg/L. Under different temperature conditions, when the initial concentration of Cd(II) exceeds 126 mg/L, the higher the temperature, the greater the uptake of Cd(II) by KBC. The maximum adsorption values were 51.67, 56.80 and 66.07 mg/g for the three temperature conditions, indicating that the increase in temperature was beneficial for adsorption.

The isothermal Langmuir and Freundlich model was used to fit the experimental data on Cd(II) adsorption by KBC nanomaterials. As can be seen from Table 3 and Fig. 5c & d, the theoretical adsorption values ($R^2 > 0.999$) calculated using the Langmuir isothermal model are close to the maximum experimental adsorption values under the range of different temperature conditions compared to the Freundlich isothermal model. This shows that the isothermal Langmuir model can better reflect the adsorption of KBC on Cd(II) and that the adsorption occurs on a homogeneous surface [27]. In addition, the maximum amount of adsorption increases with the increase of temperature for the three temperature conditions, which indicates that the adsorption process is a thermal adsorption reaction. When the kinetic and isotropic results are combined, it is clear that the Cd(II) adsorption of KBC is a process in which the chemical adsorption is increased by physical adsorption and spontaneous heat desorption and temperature increase are beneficial for adsorption.

3.3. Analysis of adsorption mechanism

Decreasing the specific surface area of BET and increasing the pore size of adsorbents after modification with potassium permanganate. SEM showed that the KBC surface became rough with significant particle binding. EDS refers to the introduction of manganese and potassium elements on the surface of KBC, together with the decrease of carbon and high oxygen elements. XRD showed that the KBC surface was charged with manganese oxides, which confirmed the SEM results and that the manganese oxide peaks in the XRD model were attenuated after Cd(II) adsorption. X-ray photoelectron spectroscopy showed that the manganese groups were introduced on the KBC surface, the Mn–O content increased after adsorption,

the –O–Cd–O-bidentate complex was formed during the adsorption process and the peak corresponding to the functional group O=CO a missing.

In short, the mechanism of Cd(II) adsorption by KBC is that increasing the pore size of potassium permanganate-modified biochar is beneficial for the physical adsorption of Cd(II). The modification facilitates the introduction of functional groups (–OH and Mn–O) on the surface of the biochar to the complex with Cd(II), and the modified biochar has a large number of polarized electrons. Thus, during the adsorption process, there is also a cation- π -electron reaction from biochar to Cd(II). The Cd(II) adsorption by KBC corresponds to the Langmuir isothermal equation and the quasi-secondary kinetic equation, and the adsorption process is a single molecule adsorption layer dominated by physical adsorption and complemented by chemical adsorption. The investigation of the diffusion model of the inner particle membrane showed that the diffusion of the particles influences the adsorption process. Thermodynamics showed that adsorption was a spontaneous process of thermal adsorption and that heating was beneficial for adsorption to continue.

4. Conclusion

The production of modified biochar nanomaterials from eucalyptus wood waste not only solves the problem of the disposal and recycling of agricultural and forestry waste, but also successfully prepares efficient heavy metal adsorption materials. Treatment with potassium permanganate increased the pore size of the biochar, introduced many polar functional groups, and generated manganese oxides in the form of MnO₂ on the surface of biochar, which was beneficial for improving the adsorption performance of biochar. Characterization analyzes and experimental studies on influencing factors showed that the mechanism of HM adsorption on biochar includes the formation of bidentate –O–Cd–O complexes on the biochar surface through oxygen- and manganese-containing groups through complexation, oxidation and cation- π -electron interactions also during the adsorption process. Thus, it is shown that the modification of the loading with potassium permanganate offers an efficient way to produce cheap biochar adsorbents for the treatment of wastewater from heavy metals.

Acknowledgments

The authors wish to acknowledge the financial support from the Science and Technology Projects of Dazhou

(Project Number: key R&D Project 2021–16) and the Doctoral Research Foundation of Dazhou Vocational and Technical College (Project Number: 2022DZYBS03).

References

- [1] E. Goretti, M. Pallottini, M.I. Ricciarini, R. Selvaggi, D. Cappelletti, Heavy metals bioaccumulation in selected tissues of red swamp crayfish: an easy tool for monitoring environmental contamination levels, *Sci. Total Environ.*, 559 (2016) 339–346.
- [2] S. Satarug, D.A. Vesey, G.C. Gobe, Current health risk assessment practice for dietary cadmium: data from different countries, *Food Chem. Toxicol.*, 106 (2017) 430–445.
- [3] S. Vasudevan, J. Lakshmi, Effect of alternating and direct current in an electrocoagulation process on the removal of cadmium from water, *Water Sci. Technol.*, 65 (2012) 353–360.
- [4] A. Izadi, A. Mohebbi, M. Amiri, N. Izadi, Removal of iron ions from industrial copper raffinate and electrowinning electrolyte solutions by chemical precipitation and ion exchange, *Miner. Eng.*, 113 (2017) 23–35.
- [5] J.A. Sirviö, M. Visanko, Lignin-rich sulfated wood nanofibers as high-performing adsorbents for the removal of lead and copper from water, *J. Hazard. Mater.*, 383 (2020) 121174, doi: 10.1016/j.jhazmat.2019.121174.
- [6] C. Zhang, Z. Yu, G. Zeng, B. Huang, H. Dong, J. Huang, Z. Yang, J. Wei, L. Hu, Q. Zhang, Phase transformation of crystalline iron oxides and their adsorption abilities for Pb and Cd, *Chem. Eng. J.*, 284 (2016) 247–259.
- [7] G. Hong, X. Li, L. Shen, M. Wang, C. Wang, X. Yu, X. Wang, High recovery of lead ions from aminated polyacrylonitrile nanofibrous affinity membranes with micro/nanostructure, *J. Hazard. Mater.*, 295 (2015) 161–169.
- [8] Faheem, H. Yu, J. Liu, J. Shen, X. Sun, J. Li, L. Wang, Preparation of MnO₂-loaded biochar for Pb²⁺ removal: adsorption performance and possible mechanism, *J. Taiwan Inst. Chem. Eng.*, 66 (2016) 313–320.
- [9] Y. Ma, W.-J. Liu, N. Zhang, Y.-S. Li, H. Jiang, G.-P. Sheng, Polyethylenimine modified biochar adsorbent for hexavalent chromium removal from the aqueous solution, *Bioresour. Technol.*, 169 (2014) 403–408.
- [10] J. Zhang, F. Lü, L. Shao, P. He, The use of biochar-amended composting to improve the humification and degradation of sewage sludge, *Bioresour. Technol.*, 168 (2014) 252–258.
- [11] Z. Chen, X. Xiao, B. Chen, L. Zhu, Quantification of chemical states, dissociation constants and contents of oxygen-containing groups on the surface of biochars produced at different temperatures, *Environ. Sci. Technol.*, 49 (2015) 309–317.
- [12] L. Ramirez Arenas, S. Ramseier Gentile, S. Zimmermann, S. Stoll, Nanoplastics adsorption and removal efficiency by granular activated carbon used in drinking water treatment process, *Sci. Total Environ.*, 791 (2021) 148175, doi: 10.1016/j.scitotenv.2021.148175.
- [13] S. Wan, N. Qu, F. He, M. Wang, G. Liu, H. He, Tea waste-supported hydrated manganese dioxide (HMO) for enhanced removal of typical toxic metal ions from water, *RSC Adv.*, 5 (2015) 88900–88907.
- [14] Z. Song, F. Lian, Z. Yu, L. Zhu, B. Xing, W. Qiu, Synthesis and characterization of a novel MnO₂-loaded biochar and its adsorption properties for Cu²⁺ in aqueous solution, *Chem. Eng. J.*, 242 (2014) 36–42.
- [15] H. Su, Z. Fang, P.E. Tsang, J. Fang, D. Zhao, Stabilisation of nanoscale zero-valent iron with biochar for enhanced transport and in-situ remediation of hexavalent chromium in soil, *Environ. Pollut.*, 214 (2016) 94–100.
- [16] X.-f. Tan, Y.-g. Liu, Y.-l. Gu, Y. Xu, G.-m. Zeng, X.-j. Hu, S.-b. Liu, X. Wang, S.-m. Liu, J. Li, Biochar-based nanocomposites for the decontamination of wastewater: a review, *Bioresour. Technol.*, 212 (2016) 318–333.
- [17] C. Sun, T. Chen, Q. Huang, J. Wang, S. Lu, J. Yan, Enhanced adsorption for Pb(II) and Cd(II) of magnetic rice husk biochar by KMnO₄ modification, *Environ. Sci. Pollut. Res.*, 26 (2019) 8902–8913.
- [18] X.-F. Tan, S.-S. Zhu, R.-P. Wang, Y.-D. Chen, P.-L. Show, F.-F. Zhang, S.-H. Ho, Role of biochar surface characteristics in the adsorption of aromatic compounds: pore structure and functional groups, *Chin. Chem. Lett.*, 32 (2021) 2939–2946.
- [19] W. Cai, J. Wei, Z. Li, Y. Liu, J. Zhou, B. Han, Preparation of amino-functionalized magnetic biochar with excellent adsorption performance for Cr(VI) by a mild one-step hydrothermal method from peanut hull, *Colloids Surf., A*, 563 (2019) 102–111.
- [20] J.M. Salleh, A.B. Nor, M.Z. Othman, Synthesis and characterization of superfine nanostructure manganese dioxide spontaneously coated onto carbon nanotubes, *Adv. Mater. Res.*, 364 (2012) 398–401.
- [21] H.-Y. Wang, P. Chen, Y.-G. Zhu, K. Cen, G.-X. Sun, Simultaneous adsorption and immobilization of As and Cd by birnessite-loaded biochar in water and soil, *Environ. Sci. Pollut. Res.*, 26 (2019) 8575–8584.
- [22] J. Liang, X. Li, Z. Yu, G. Zeng, Y. Luo, L. Jiang, Z. Yang, Y. Qian, H. Wu, Amorphous MnO₂ modified biochar derived from aerobically composted swine manure for adsorption of Pb(II) and Cd(II), *ACS Sustainable Chem. Eng.*, 5 (2017) 5049–5058.
- [23] S.O. Amusat, T.G. Kebede, S. Dube, M.M. Nindi, Ball-milling synthesis of biochar and biochar-based nanocomposites and prospects for removal of emerging contaminants: a review, *J. Water Process Eng.*, 41 (2021) 101993, doi: 10.1016/j.jwpe.2021.101993.
- [24] Q. Du, J. Sun, Y. Li, X. Yang, X. Wang, Z. Wang, L. Xia, Highly enhanced adsorption of Congo red onto graphene oxide/chitosan fibers by wet-chemical etching off silica nanoparticles, *Chem. Eng. J.*, 245 (2014) 99–106.
- [25] J. Wu, T. Wang, J. Wang, Y. Zhang, W.-P. Pan, A novel modified method for the efficient removal of Pb and Cd from wastewater by biochar: enhanced the ion exchange and precipitation capacity, *Sci. Total Environ.*, 754 (2021) 142150, doi: 10.1016/j.scitotenv.2020.142150.
- [26] L.D. Puppa, M. Komárek, F. Bordas, J.-C. Bollinger, E. Joussein, Adsorption of copper, cadmium, lead and zinc onto a synthetic manganese oxide, *J. Colloid Interface Sci.*, 399 (2013) 99–106.
- [27] S. Zhu, M.A. Khan, F. Wang, Z. Bano, M. Xia, Rapid removal of toxic metals Cu²⁺ and Pb²⁺ by amino trimethylene phosphonic acid intercalated layered double hydroxide: a combined experimental and DFT study, *Chem. Eng. J.*, 392 (2020) 123711, doi: 10.1016/j.cej.2019.123711.